Journal of Applied Electrochemistry **33**: 619–625, 2003.

Effects of the stoichiometric ratio of aluminium and manganese on electrochemical properties of hydrogen storage alloys

M.-S. WU[1,*], H.-R. WU[2], Y.-Y. WANG[2] and C.-C. WAN[2]
[1]*Materials Research Laboratories, Industrial Technology Research Institute, Hsinchu, 310, Taiwan, ROC*
[2]*Department of Chemical Engineering, National Tsing-Hua University, Hsinchu, 300, Taiwan, ROC*
*(*author for correspondence, fax: +886 3 5820442, e-mail: ms_wu@url.com.tw)*

Received 13 October 2002; accepted in revised form 4 April 2003

Key words: enthalpy change, hydrogen storage alloys, pressure-composition isotherm

Abstract

With the aim of enhancing the capacity and electrochemical performances of hydrogen-storage alloy electrodes, $MmM_{4.3}(Al_{0.3}Mn_{0.4})_x$ (Mm = La-rich mischmetal, M = Ni, Co) alloys were investigated. $MmM_{4.3}(Al_{0.3}Mn_{0.4})_x$ alloys possessing appropriate plateau pressure and high storage capacity can be obtained by adjusting the stoichiometric ratio of Al–Mn (x value). In this situation, the unit cell volumes increase with increasing x and the enthalpy changes of hydride formation decrease with increasing x, thereby changing the alloy properties in the gas phase and the electrochemical environment. The plateau pressure and the charge potential both increase with decreasing x. The x value influences the surface states and bulk properties. When x is lower than 0.5, both the charge-transfer reaction on the alloy surface and the diffusion resistance within the bulk alloy are much improved. High-rate dischargeability at high current density is controlled mainly by the limiting current density. $MmM_{4.3}(Al_{0.3}Mn_{0.4})_{0.5}$ alloy, having the highest storage capacity and good electrochemical performance, is an appropriate candidate for battery materials.

1. Introduction

Rechargeable nickel-metal hydride batteries with hydrogen storage alloy as the negative electrode material have been used extensively because of their several advantages: high energy density, good high-rate dischargeability, long cycle life and environmental acceptability. In addition, the performance of hydrogen storage alloys has improved remarkably through surface modifications. To improve surface properties, several alkaline processes have been proposed [1–4]. Microencapsulation of the alloy powder with various kinds of electroless coating like Cu, Ni–P, Ni–B and Ni has also produced effective improvement in cycle life [5–10].

Other than surface properties, bulk composition is also an important factor in the electrochemical performance of alloy electrodes. Aluminium and manganese have been confirmed to be effective in improving the performance of hydrogen-storage alloy electrodes [11–14]. It is generally accepted that adding aluminium to hydrogen storage alloy can reduce the equilibrium pressure plateau and prolong cycle life in AB_5-type hydrogen storage alloys. However, one drawback is the decrease in hydrogen storage capacity, which results from the displacement of Ni atoms by larger Al atoms on the 3g site, consequently reducing the sites available for hydrogen storage [11, 12]. Mendelsohn et al. [13] stated that the aluminium additions were there to reduce greatly the plateau pressure of the $ANi_{5-x}Al_x$ (A = La, cerium-free mischmetal) hydride compared with that of the corresponding ANi_5 hydride. If the plateau pressure is low, poor discharge efficiency is an end result. Iwakura et al. [11] found that manganese enhances discharge capacity and high-rate dischargeability of alloy electrodes. Machida et al. [14] pointed out that the extent of the plateau region in pressure–composition isotherms depends remarkably on the Mn content. In technical terms, length of the plateau corresponds to the hydrogen storage capacity of the system. Generally, equilibrium hydrogen pressures of alloy electrodes are not very high, because low charging efficiencies induce hydrogen evolution reaction (HER) and result in low capacities. The appropriate equilibrium pressure generally lies between 10^{-3} and 1 atm [15].

Based on these studies, the main function of Al is to regulate the plateau pressure and the function of Mn is to affect the length of plateau pressure in pressure-composition isotherms. Thus, it would be useful to combine these two elements to obtain high performance alloys. In this paper, the stoichiometric ratio of Al and Mn in $MmM_{4.3}(Al_{0.3}Mn_{0.4})_x$ alloys was adjusted to an appropriate plateau pressure and high storage capacity. Electrochemical properties of hydrogen storage alloy

with different stoichiometric ratios of Mn and Al were also investigated.

2. Experimental details

Hydrogen storage powder $MmM_{4.3}(Al_{0.3}Mn_{0.4})_x$ (Mm = La-rich mischmetal, M = Ni, Co) was prepared by mechanical pulverization to a particle size of less than 250 mesh. The powder was mixed with 3 wt % polytetrafluoroethylene (PTFE) and pasted onto a foamed nickel screen, then pressed at 1000 kg cm^{-2} and dried at 150 °C for 60 min. The resultant electrode dimension was 2 cm × 2 cm × 0.08 cm.

Each test cell comprised of a working electrode, a NiOOH-counter electrode (made of nickel hydroxide powder) and a reference electrode (Hg/HgO electrode). Capacity of the counter electrode was much larger than that of the working electrode so the measured capacity was determined completely by the latter. A working electrode wrapped with non-woven polypropylene (PP) separator was inserted between two counter electrodes. Electrodes were tightly bound in a Teflon holder. Galvanostatic charge/discharge cycles were applied in 30 wt % KOH solution at 30 °C. Test cells were charged for 8 h and discharged to −0.7 V vs Hg/HgO at a constant current density of 50 mA g^{-1}. Anodic polarization measurements were performed at 30 °C with a potentiostat (Schlumberger SI 1286), scan rate 1 mV s^{-1}. Test cells were activated first then charged at 50 mA g^{-1} for 2 h prior to any measurements.

P–C–T (pressure–composition isotherms) for hydrogen absorption and desorption were measured by the Sievert method. About 5 grams of the same powder were taken for each run. For activation, alloy powder was evacuated and exposed to hydrogen atmosphere at 5 kg cm^{-2} and heated at 350 °C for 1.5 h. This was followed by dehydriding the powder by evacuating and heating at 350 °C for 2.5 h. After two cycles of activation, absorption P–C–T data was recorded.

Surface morphology of the powder was examined with a scanning electron microscope (JSM 840A). The crystal structure of the alloy powder was identified by using X-ray diffraction (XD-5) with a CuK_α radiation.

3. Results and discussion

3.1. *Crystallographic and thermodynamic properties*

Hydrogen storage alloys, $MmM_{4.3}(Al_{0.3}Mn_{0.4})_x$ (x = 0.25, 0.5, 0.75 and 1.0), were investigated to search for the most suitable proportion used in a metal–hydride battery system. The influences of x on the alloy structure were examined by XRD. Figure 1 shows the XRD patterns of $MmM_{4.3}(Al_{0.3}Mn_{0.4})_x$ alloys. The same structure can be observed in all cases, except where diffraction peaks shift to smaller angles as x increases. All peaks were assigned to the hexagonal $CaCu_5$ type structure [16]. This means that the main structure in $MmM_{4.3}(Al_{0.3}Mn_{0.4})_x$ alloys can not be changed by adjusting the stoichiometric ratio of Al and Mn. The shifted XRD peak positions are used to obtain unit cell lattice parameters and volumes, and the results are shown in Figure 2. Apparently, lattice volume is increased by increasing x. Lattice volume may affect the reaction of hydrogen to metal. Figure 2 also shows the enthalpy changes (ΔH) of $MmM_{4.3}(Al_{0.3}Mn_{0.4})_x$ alloys. Enthalpy changes in hydride formations are calculated by the van't Hoff equation with data from P–C–T curves at various temperatures [17]. From the Figure, it is clear that enthalpy change increases negatively with increasing x, and this matches the increasing tendency of the unit cell volume. Iwakura et al. [11] investigated the

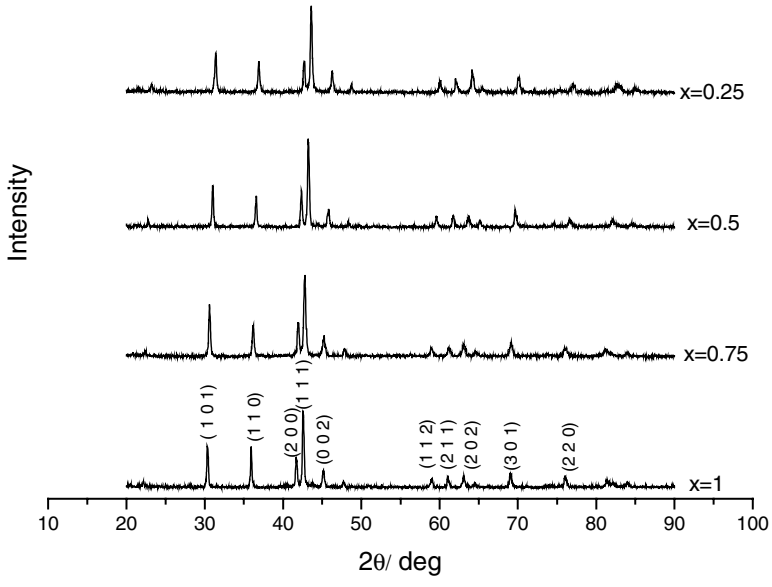

Fig. 1. XRD patterns for $MmM_{4.3}(Al_{0.3}Mn_{0.4})_x$ alloys.

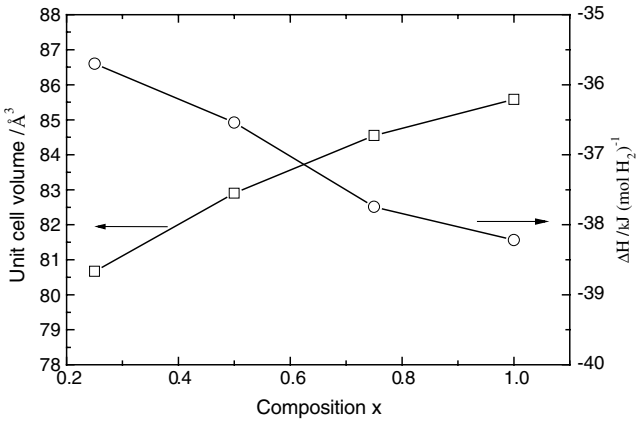

Fig. 2. Unit cell volumes and enthalpy changes of $MmM_{4.3}$-$(Al_{0.3}Mn_{0.4})_x$ alloys.

$MmNi_{5-x}Al_x$ alloys, also finding similar results. Because aluminium has a larger metallic bond radius than nickel, the stability of hydrides increases with increasing aluminium content.

3.2. *PCT curve measurements*

To understand the hydrogen absorption characteristics of $MmM_{4.3}(Al_{0.3}Mn_{0.4})_x$ alloys, pressure-composition isotherms were measured in the gas phase at 40 °C, as shown in Figure 3. It is clear that the equilibrium pressure plateaus are sensitive to the stoichiometric ratio of Mn and Al, and they decrease with increasing x. In general, a plateau pressure higher than that of the cell pressure would cause a decrease in charging efficiency due to the hydrogen evolution reaction (HER), while a plateau pressure lower than 10^{-3} atm would cause a decrease in discharging efficiency, primarily due to the formation of a more stable metal-hydride which is rather difficult to discharge. It is desirable to have the plateau pressure lie between 10^{-3} and 1 atm in the temperature range of −20 to 60 °C [15].

Thermodynamic properties of alloys may be used to explain how plateau pressures depend on composition. The plateau pressures in Figure 3 depend on enthalpy changes: that is, the lower the enthalpy change, the lower the plateau pressure. In alloys with higher ΔH, metal-to-hydrogen bond strengths are weak, and hydrogen can not react with the alloy, resulting in hydrogen evolution reaction. However, in alloys with lower ΔH, the bonds are strong and the alloys react with hydrogen to form more stable hydrides which are incapable of storing hydrogen reversibly [18]. As mentioned above, unsuitable plateau pressures can lead to detrimental effects in charging and discharging. Therefore, a major problem is determining the enthalpy change, which provides a suitable plateau pressure. According to Ovshinsky et al. [18], an alloy is suitable for battery applications if the enthalpy change is between −25.2 and −50.4 kJ (mol H_2)$^{-1}$. For $x = 0.25$, 0.5, 0.75 and 1.0, the enthalpy changes of $MmM_{4.3}(Al_{0.3}Mn_{0.4})_x$ alloys are −35.7, −36.5, −37.7 and −38.2 kJ mol^{-1}, respectively. Therefore, $MmM_{4.3}(Al_{0.3}Mn_{0.4})_x$ alloys are potential candidates for electrode materials.

3.3. *Electrode capacity measurements*

The electrochemical absorption and desorption of a hydrogen-storage alloy electrode, Me, in an alkaline solution can be expressed as follows [19]:

$$Me + y\,H_2O + y\,e^- \rightleftharpoons MeH_y + y\,OH^- \qquad (1)$$

so that each absorbed/desorbed hydrogen atom corresponds to the storage of one electrode. When a fully charged electrode is electrochemically discharged, the discharge capacity, C_d (mAh g^{-1}) is calculated using Equation 2 [20, 21]:

$$C_d = \frac{n[(H/Me)_{10} - (H/Me)_{0.01}]F}{3.6W_M} \qquad (2)$$

where n is the number of metallic atoms per formula unit of alloy, $(H/Me)_{10}$ and $(H/Me)_{0.01}$ are atomic ratios

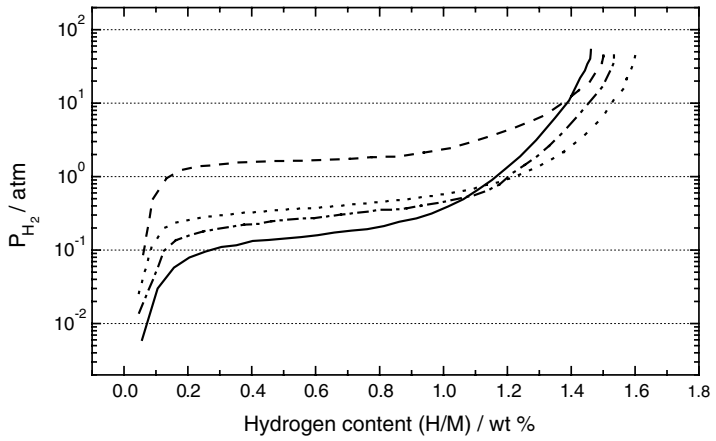

Fig. 3. Pressure–composition isotherms for $MmM_{4.3}(Al_{0.3}Mn_{0.4})_x$ alloys at 40 °C. Key: (- - -) $x = 0.25$, (···) $x = 0.50$, (-·-·-) $x = 0.75$, (—) $x = 1.00$.

Table 1. Theoretical capacities calculated from Equation 2 and electrochemical discharge capacities

Materials	H/M /wt %	Theoretical capacity /mAh g^{-1}	Actual capacity /mAh g^{-1}
$MmM_{4.3}(Al_{0.3}Mn_{0.4})_{0.25}$	1.30	348	260
$MmM_{4.3}(Al_{0.3}Mn_{0.4})_{0.5}$	1.50	401	291
$MmM_{4.3}(Al_{0.3}Mn_{0.4})_{0.75}$	1.40	376	275
$MmM_{4.3}(Al_{0.3}Mn_{0.4})_{1.0}$	1.34	360	252

of hydrogen to metal at the equilibrium hydrogen pressure of 10 and 0.01 atm, F is the faradaic constant, and W_M the molecular weight of the active electrode material.

Values of the theoretical capacities from Equation 2 and the electrochemical discharge capacities are summarized in Table 1. Here, different hydrogen storage capacities are measured by the length of equilibrium pressure plateau in the range 0.01 to 10 atm, whereas electrochemical discharge capacity is taken to be the maximum capacity achieved during cycling of the cell. For $x = 0.25$, 0.5, 0.75 and 1.0, the actual capacities of $MmM_{4.3}(Al_{0.3}Mn_{0.4})_x$ are 260, 291, 275 and 252 mAh g^{-1}, respectively. These results are in fair agreement with the orders of theoretical capacities. Note that the hydrogen stored electrochemically in each of the electrode samples is much lower than that stored via gas phase absorption. One possible explanation is that the electrochemical capacity depends greatly on the electrode characteristics and cell type, since it is believed that different methods of making electrodes result in different discharge capacities. In addition, factors like particle size, electrode thickness, conducting agent, binder and electrolyte can also influence electrode characteristics.

3.4. *Charge characteristics*

Appropriate electrochemical potentials for hydriding/dehydriding an alloy electrode are determined from the equilibrium hydrogen pressure of metal hydrides with the Nernst equation. For a cell containing 6 M KOH electrolyte at 20 °C and 1 atm, the Nernst equation can be written as [22]

$$E_o = -0.9324 - 0.0291 \log(P_{H_2}) \quad (3)$$

where E_o (vs Hg/HgO) represents the equilibrium potential of the MeH_x electrode, and P_{H_2} is the equilibrium hydrogen pressure. Potential changes in Equation 3 are only about 29 mV (decade)$^{-1}$ of variation in hydrogen pressure. Hence, the equilibrium potential should be held at about −0.9324 V during either the hydriding or the dehydriding process.

Figure 4 shows the potential curves of $MmM_{4.3}(Al_{0.3}Mn_{0.4})_x$ alloy electrodes during charging. An inversely proportional relationship exists between the overpotential $(E - E_o)$ and the x value. Comparing

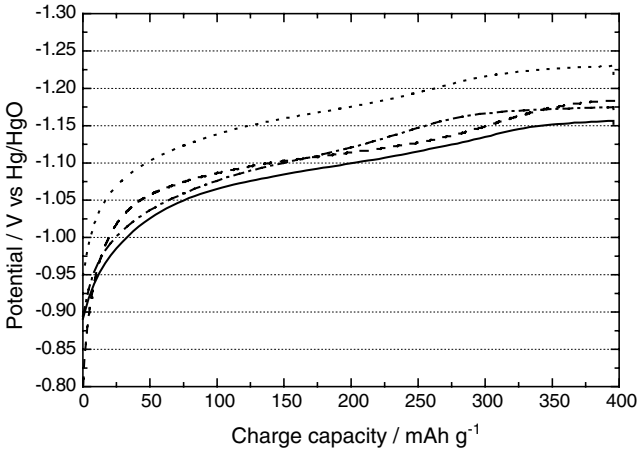

Fig. 4. Potential curves of $MmM_{4.3}(Al_{0.3}Mn_{0.4})_x$ alloy electrodes during charging. Key: (····) $x = 0.25$, (- - -) $x = 0.50$, (-·-·-) $x = 0.75$, (—) $x = 1.00$.

Figure 3 with Figure 4, these alloys have similar trends in both plateau pressures and charge potentials, and charge potential is higher when the plateau pressure increases. Clearly, alloys with $x \geqslant 0.5$ have suitable and similar charge potentials, and the alloy with $x = 0.25$ has the highest charge potential. In this case, the strength of metal to hydrogen bond is weak (large ΔH). The competing hydrogen evolution reaction (HER) is favoured over hydrogen absorption where hydrogen gas is formed at the electrode surface leading to a decrease in charging efficiency. This is the reason why the $MmM_{4.3}(Al_{0.3}Mn_{0.4})_{0.25}$ alloy has lower electrochemical capacity than $MmM_{4.3}(Al_{0.3}Mn_{0.4})_{0.5}$. Therefore, enthalpy change plays an important role in the charging efficiency of the alloy electrode. Poor charging efficiency can lead to a build-up of pressure during the charge/discharge cycle. Therefore alloy electrodes with higher charge efficiencies are essential to sealed-type batteries.

3.5. *Electrochemical properties*

Another consideration in the use of alloy materials in nickel-metal hydride batteries relates to electrochemical kinetics and transport process [18]. For electrochemical kinetic studies, anodic polarization curves for the alloy electrodes were obtained by linear sweep voltammetry (LSV). The anodic current (i) in general increases with overpotential, but when strongly polarized, a limiting current (i_L) can result from the mass transport limitation of some species. The main species are hydrogen atoms in the bulk alloy, hydroxyl ions (OH^-) in the electrolyte, or water molecules (H_2O) in solution. In this study, cells were designed to contain excess electrolyte (30 wt % KOH, highly flooded) so that a reasonable assumption is that the diffusion resistance of OH^- and H_2O is negligible compared with that of hydrogen atoms. The anodic overpotential (η) can be expressed as [17, 23]

$$\eta = \frac{RT}{(1-\alpha)F}\ln\left(\frac{i}{i_o}\right) + \frac{RT}{(1-\alpha)F}\ln\left(\frac{i_L}{i_L - i}\right) \quad (4)$$

where F is the faradaic constant, R the gas constant, T the temperature and α the transfer coefficient. The first term on the right-hand side of Equation 4 is the activation overpotential due to charge transfer resistance. The second term corresponds to the concentration overpotential due to the diffusion resistance of hydrogen transport. Rearranging Equation 4 yields the following expression:

$$\eta = \frac{RT}{(1-\alpha)F}\ln\left(\frac{i_L}{i_o}\right) + \frac{RT}{(1-\alpha)F}\ln\left(\frac{i}{i_L - i}\right) \quad (5)$$

According to Equation 5, a plot of η against $\ln(i/i_L - i)$ should produce a straight line of slope $RT/(1-\alpha)F$ and intercept $RT/(1-\alpha)F \times \ln(i_L/i_o)$. Hence, α and i_o can be calculated from i_L and T. Figure 5 shows the anodic polarization curves of $MmM_{4.3}(Al_{0.3}Mn_{0.4})_x$ alloy electrodes. The corresponding electrochemical kinetic parameters are listed in Table 2. Alloy electrodes with large i_o are responsible for low charge transfer resistance. It can be seen that the exchange current densities and limiting current densities increase with decreasing x. Both i_o and i_L depend on hydrogen concentration within the bulk alloy. To neglect hydrogen concentration on the kinetics data, all alloy electrodes were charged at about 50 mA g^{-1} for 2 h prior to LSV measurements. For $x = 0.25$, 0.5, 0.75 and 1.0, i_o values are 134.6, 120.8, 100 and 89.0 mA g^{-1}, respectively. It is generally believed that exchange current densities are related to surface properties, such as oxide thickness, electric conductivity, surface porosity, topology, surface area, and degree of catalytic activity [18]. As a result, better surface properties of $MmM_{4.3}(Al_{0.3}Mn_{0.4})_x$ alloy electrodes can be obtained by adjusting the x value to be lower than 0.5. On the other hand, limiting current densities are dependent on hydrogen diffusion in the bulk alloy. The values of i_L for $x = 0.25$, 0.5, 0.75 and 1.0 are 1220.7, 1208.4, 996.2 and 874.2 mA g^{-1}, respectively. An alloy electrode has a lower diffusion resistance if its x is lower than 0.5. In comparison with i_L and ΔH, it can be seen that the lower the ΔH is, the lower the i_L will be. In many cases, an alloy absorbing large amounts of hydrogen has higher diffusion resistance to hydrogen release due to the forming of a more stable hydride (lower ΔH) and vice versa. This is the reason that the $MmM_{4.3}(Al_{0.3}Mn_{0.4})_1$ alloy has the lowest i_L ($\Delta H = -38.2$ kJ mol^{-1}). Since the value of ΔH is an index for the metal–hydrogen bonding strength, not only does it determine the capacity of hydrogen absorption but it also controls the diffusion resistance to hydrogen release during discharge. It is reasonable to claim that ΔH is a major factor in the charge–discharge performance of metal-hydride electrodes. Based on LSV data, the stoichiometric ratio of Al and Mn influences the surface states and bulk properties. When x is lower than 0.5, both the charge-transfer reaction on the alloy surface and diffusion resistance within the bulk alloy can be much improved.

Table 2. Electrochemical kinetic parameters of $MmM_{4.3}(Al_{0.3}Mn_{0.4})_x$ alloy electrodes

Materials	Exchange current density, i_o/mA g^{-1}	Limiting current density, i_L/mA g^{-1}	Transfer coefficient, α
$MmM_{4.3}(Al_{0.3}Mn_{0.4})_{0.25}$	134.6	1220.7	0.67
$MmM_{4.3}(Al_{0.3}Mn_{0.4})_{0.5}$	120.8	1208.4	0.64
$MmM_{4.3}(Al_{0.3}Mn_{0.4})_{0.75}$	100.0	996.2	0.58
$MmM_{4.3}(Al_{0.3}Mn_{0.4})_1$	89.0	874.2	0.56

The percentage high-rate dischargeability (HRD), which is another important factor in practical use, can be defined as [24]

$$\mathrm{HRD} = \frac{C_x}{C_x + C_{50}} \times 100$$

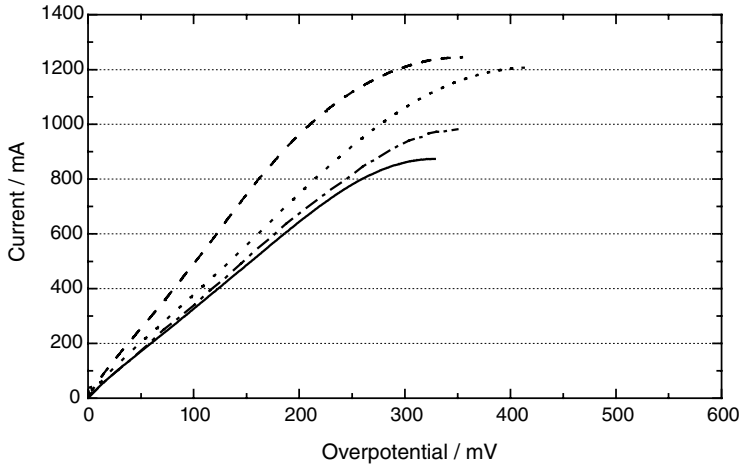

Fig. 5. Anodic polarization curves for $MmM_{4.3}(Al_{0.3}Mn_{0.4})_x$ alloy electrodes. Key: (- - -) $x = 0.25$, (···) $x = 0.50$, (-·-·) $x = 0.75$, (—) $x = 1.00$.

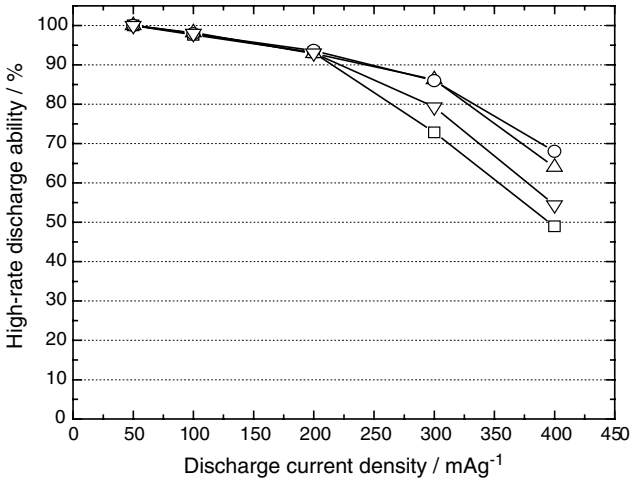

Fig. 6. Relationship between discharge current densities and high-rate dischargeabilities for $MmM_{4.3}(Al_{0.3}Mn_{0.4})_x$ alloy electrodes. Key: (○) $x = 0.25$, (△) $x = 0.5$, (▽) $x = 0.75$, (□) $x = 1.00$.

where C_x indicates the discharge capacity at x mA g^{-1}, and C_{50} is the residual discharge capacity determined at 50 mA g^{-1} by resting 30 min after the measurement of C_x.

Figure 6 shows the relationships between discharge current densities and high-rate dischargeabilities for $MmM_{4.3}(Al_{0.3}Mn_{0.4})_x$ alloy electrodes. Clearly, high-rate dischargeabilities increase with decreasing x. Among these electrodes, the one with $x = 0.25$ has the best HRD; which can be seen from the comparisons that for $x = 1$, $x = 0.75$, $x = 0.5$, and $x = 0.25$ at 400 mA g^{-1}, HRD are 48, 55, 65 and 68%, respectively. HRD is controlled by the rate of charge transfer (i_o) on an alloy surface or the hydrogen diffusion (i_L) in the alloy itself [17, 24]. If the electrochemical reaction on the surface is rate-determining, then there exists a linear dependence between the high-rate dischargeability and the exchange current density. In contrast, if hydrogen diffusion in the crystal lattice is rate-determining, the high-rate dischargeability is independent of the exchange current density and hence remains constant [11]. Figure 7 shows the relationship between high-rate

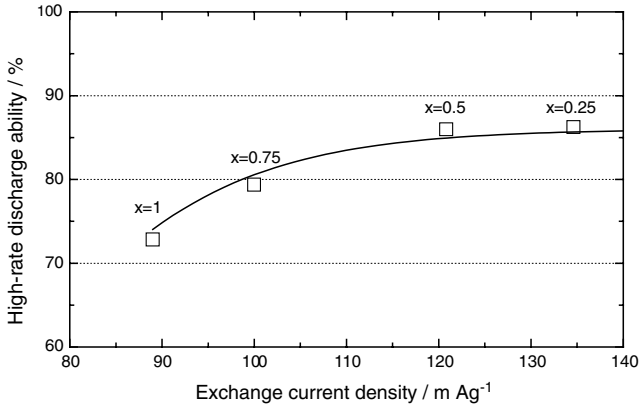

Fig. 7. Relationship between high-rate dischargeabilities and exchange current densities for $MmM_{4.3}(Al_{0.3}Mn_{0.4})_x$ alloy electrodes.

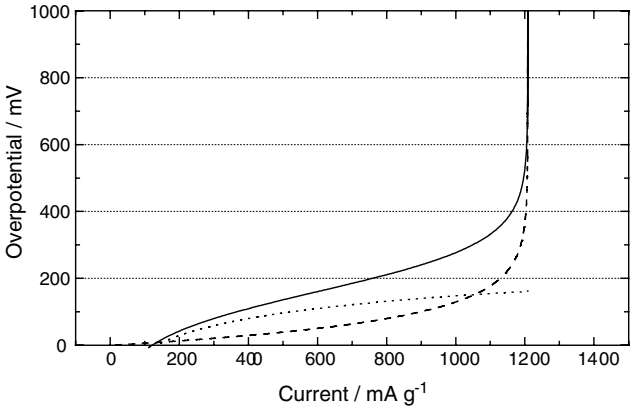

Fig. 8. Relationship between overpotential and discharge current density for the $MmM_{4.3}(Al_{0.3}Mn_{0.4})_{0.5}$ alloy electrode. Key: (···) activation overpotential; (- - -) concentration overpotential; (—) total overpotential.

dischargeabilities and exchange current densities for the $MmM_{4.3}(Al_{0.3}Mn_{0.4})_x$ alloy electrodes. Clearly, for x lower than 0.5, the high-rate dischargeability remains constant, which implies that the diffusion of hydrogen in the alloy is rate-determining. $MmM_{4.3}(Al_{0.3}Mn_{0.4})_{0.25}$ and $MmM_{4.3}(Al_{0.3}Mn_{0.4})_{0.5}$ alloys have higher limiting current densities, and consequently they exhibit good high-rate dischargeabilities. This is consistent with results reported by Iwakura et al. [11], in whose studies of $MmNi_{5-x}Al_x$ alloy electrode, high-rate dischargeabilities were found to be almost constant for x over 0.4.

To distinguish the contribution of charge transfer from mass transfer resistance, Equation 4 is employed to calculate the anodic concentration overpotential (η_c) and activation overpotential (η_a) during discharge. Figure 8 illustrates the relationship between overpotential and discharge current density for $MmM_{4.3}(Al_{0.3}Mn_{0.4})_{0.5}$ alloy electrode. When the polarization current is larger than the exchange current density, electrochemical reactions are controlled by the charge-transfer reaction (η_a) and mass transfer processes (η_c). Figure 8 shows that η_a is greater than η_c at low discharge current densities and vice versa. This means that the release of hydrogen in bulk is the rate-determining step for metal hydride in high rate discharge. According to hydrogen storage capacities and electrochemical characteristics of $MmM_{4.3}(Al_{0.3}Mn_{0.4})_x$ ($x = 0.25$, 0.5, 0.75 and 1.0) alloy electrodes, satisfactory high-rate dischargeabilities can be found by adjusting x to be lower than 0.5; but the storage capacity for $x = 0.25$ is much lower than that of $x = 0.5$. Therefore, $MmM_{4.3}(Al_{0.3}Mn_{0.4})_{0.5}$ alloy is a better choice for use as a battery material.

4. Conclusions

$MmM_{4.3}(Al_{0.3}Mn_{0.4})_x$ alloys were investigated for use as electrode materials. Plateau pressure increases with

decreasing x for the alloys in gas-phase reaction. Factors affecting this phenomenon are lattice structure and enthalpy change in hydride formation. High plateau pressure from high enthalpy change (ΔH) is due to the weak metal-to-hydrogen bond and vice versa. All $MmM_{4.3}(Al_{0.3}Mn_{0.4})_x$ alloys have similar trends both in plateau pressure and charge potential. The contribution of charge-transfer potential (η_a) and mass-transfer overpotential (η_c) to alloy electrodes during discharge can be easily derived from anodic polarization data. η_c is lower than η_a, at low discharge current densities and becomes more dominant at higher current densities. High-rate dischargeability at high current density is mainly controlled by limiting the current density rather than the exchange current density. From gas-phase measurements, $MmM_{4.3}(Al_{0.3}Mn_{0.4})_{0.5}$ alloy is determined to have the highest storage capacity and a moderate plateau pressure. In addition, it shows good electrochemical performance, especially in high-rate dischargeability. In conclusion, $MmM_{4.3}(Al_{0.3}Mn_{0.4})_{0.5}$ alloy is a good prospective candidate for battery materials.

References

1. H.H. Uchida, Y. Watamabe, Y. Matsumura and H. Uchida, *J. Alloys Compd.* **231** (1995) 679.
2. W.K. Choi, K. Yamataka, S.G. Zhang, H. Inoue and C. Iwakura, *J. Electrochem. Soc.* **146** (1999) 46.
3. C. Iwakura, W.K. Choi, S.G. Zhang and H. Inoue, *Electrochim. Acta* **44** (1999) 1677.
4. D. Yan, G. Sandrock and S. Suda, *J. Alloys Compd.* **216** (1994) 237.
5. T. Sakai, H. Ishikawa, K. Oguro, C. Iwakura and H. Yoneyama, *J. Electrochem. Soc.* **134** (1987) 558.
6. C.Jun and Z. Yunshi, *Int. J. Hydrogen Energy* **20** (1995) 235.
7. J.L. Luo and N. Cui, *J. Alloys Compd.* **264** (1998) 299.
8. J. Chen, D.H. Bradhurst, S.X. Dou and H.K. Liu, *J. Alloys Compd.* **280** (1998) 290.
9. S.N. Jenq, H.W. Yang, Y.Y. Wang and C.C. Wan, *J. Power Sources* **57** (1995) 111.
10. M.S. Wu, H.R. Wu, Y.Y. Wang and C.C. Wan, *J. Alloys Compd.* **302** (2000) 248.
11. C. Iwakura, T. Oura, H. Inoue and M. Matsuoka, *Electrochim. Acta* **41** (1996) 117.
12. A. Percheron-Guegan, C. Lartigue, J.C. Achard, P. Germi and F. Tasset, *J. Less-Common Met.* **74** (1980) 1.
13. M.H. Mendelsohn, D.M. Gruen and A.E. Dwight, *J. Less-Common Met.* **63** (1979) 193.
14. Y. Machida, T. Yamadaya and M. Asanuma, *in* A.F Andresen and A.J. Maeland (Eds), International. Symposium on 'Hydrides for Energy Storage' (Geilo, Norway, 1977), p. 329.
15. T. Sakai, K. Muta, H. Miyamura, N. Kuriyama and H. Ishikawa, *in* D.A. Corrigan and S. Srinivasan (Eds), Proceedings of the Symposium on 'Hydrogen Storage Materials, Batteries, and Electrochemistry', **PV92-5**. (The Electrochemical Society, Pennington, NJ, 1992), p. 59.
16. N. Higashiyama, Y. Matsuura, H. Nakamura, M. Kimoto, M. Nogami, I. Yonezu and K. Nishio, *J. Alloys Compd.* **253–254** (1997) 648.
17. H.W. Yang, Y.Y. Wang and C.C. Wan, *J. Electrochem. Soc.* **143** (1996) 429.
18. S.R. Ovshinsky, M.A. Fetcenko and J. Ross, *Science* **260** (1993) 176.
19. C. Jordy, A. Percheron-Guegan, J. Bouet, P. Sanchez, C. Chanson and J. Leonardi, *J. Less-Common Met.* **172–174** (1991) 1236.
20. A. Anani, A. Visintin, S. Srinivasan and A.J. Appleby, *in* D.A. Corrigan and S. Srinivasan (Eds), ref. [15], p. 105.
21. C. Iwakura, M. Matsuoka, K. Asai and T. Kohno, *J. Power Sources* **38** (1992) 355.
22. C. Iwakura, Y. Kajiya, H. Yoneyama, T. Sakai, K. Oguro and H. Ishikawa, *J. Electrochem. Soc.* **136** (1989) 1351.
23. M. Geng, J. Han, F. Feng and D.O. Northwood, *J. Electrochem. Soc.* **146** (1999) 3591.
24. M. Matsuoka, K. Asai, Y. Fukumoto and C. Iwakura, *Electrochim. Acta* **38** (1993) 659.